

RESEARCH ARTICLE

Plasmodium vivax populations in the western Greater Mekong Subregion evaluated using a genetic barcode

Yubing Hu¹ , Yuling Li^{1,2} , Awtum M. Brashear³, Weilin Zeng⁴, Zifang Wu¹, Lin Wang¹, Haichao Wei¹, Myat Thu Soe⁵, Pyae Linn Aung⁵, Jetsumon Sattabongkot⁶, Myat Phone Kyaw⁵, Zhaoqing Yang⁴, Yan Zhao^{1*}, Liwang Cui^{3*}, Yaming Cao^{1*} 

1 Department of Immunology, College of Basic Medical Sciences, China Medical University, Shenyang, Liaoning, China, **2** Emergency Department, The First Affiliated Hospital of Dalian Medical University, Dalian, Liaoning, China, **3** Division of Infectious Disease and International Medicine, Department of Internal Medicine, Morsani College of Medicine, University of South Florida, Tampa, Florida, United States of America, **4** Department of Pathogen Biology and Immunology, Kunming Medical University, Kunming, China, **5** Myanmar Health Network Organization, Yangon, Myanmar, **6** Mahidol Vivax Research Unit, Faculty of Tropical Medicine, Mahidol University, Bangkok, Thailand

 These authors contributed equally to this work.

* yzhao90@cmu.edu.cn (YZ); liwangcui@usf.edu (LC); ymcao@cmu.edu.cn (YC)



OPEN ACCESS

Citation: Hu Y, Li Y, Brashear AM, Zeng W, Wu Z, Wang L, et al. (2024) *Plasmodium vivax* populations in the western Greater Mekong Subregion evaluated using a genetic barcode. *PLoS Negl Trop Dis* 18(7): e0012299. <https://doi.org/10.1371/journal.pntd.0012299>

Editor: Karin Kirchgatter, SUCEN/IMT/USP, BRAZIL

Received: February 5, 2024

Accepted: June 18, 2024

Published: July 3, 2024

Copyright: © 2024 Hu et al. This is an open access article distributed under the terms of the [Creative Commons Attribution License](https://creativecommons.org/licenses/by/4.0/), which permits unrestricted use, distribution, and reproduction in any medium, provided the original author and source are credited.

Data Availability Statement: The data used for analysis have been listed in the [Supporting Information](#) as [S1 Dataset](#).

Funding: This work received funding from the National Institute of Allergy and Infectious Diseases (U19 AI089672 to LC), National Institute of Health, USA. The funders had no role in study design, data collection and analysis, decision to publish, or preparation of the manuscript.

Competing interests: The authors have declared that no competing interests exist.

Abstract

An improved understanding of the *Plasmodium vivax* populations in the Great Mekong Subregion (GMS) is needed to monitor the progress of malaria elimination. This study aimed to use a *P. vivax* single nucleotide polymorphism (SNP) barcode to evaluate the population dynamics and explore the gene flow among *P. vivax* parasite populations in the western GMS (China, Myanmar and Thailand). A total of 315 *P. vivax* patient samples collected in 2011 and 2018 from four regions of the western GMS were genotyped for 42 SNPs using the high-throughput MassARRAY SNP genotyping technology. Population genetic analysis was conducted to estimate the genetic diversity, effective population size, and population structure among the *P. vivax* populations. Overall, 291 samples were successfully genotyped at 39 SNPs. A significant difference was observed in the proportion of polyclonal infections among the five *P. vivax* populations ($P = 0.0012$, Pearson Chi-square test, $\chi^2 = 18.1$), with western Myanmar having the highest proportion (96.2%, 50/52) in 2018. Likewise, the average complexity of infection was also highest in western Myanmar (1.31) and lowest in northeast Myanmar (1.01) in 2018. The older samples from western China in 2011 had the highest pairwise nucleotide diversity (π , 0.388 ± 0.046), expected heterozygosity (H_e , 0.363 ± 0.02), and the largest effective population size. In comparison, in the neighboring northeast Myanmar, the more recent samples in 2018 showed the lowest values (π , 0.224 ± 0.036 ; H_e , 0.220 ± 0.026). Furthermore, the 2018 northeast Myanmar parasites showed high and moderate genetic differentiation from other populations with F_{ST} values of 0.162–0.252, whereas genetic differentiation among other populations was relatively low ($F_{ST} \leq 0.059$). Principal component analysis, phylogeny, and STRUCTURE analysis showed that the *P. vivax* population in northeast Myanmar in 2018 substantially diverged from other populations. Although the 42 SNP barcode is a valuable tool for tracking parasite origins of

worldwide parasite populations, a more extended barcode with additional SNPs is needed to distinguish the more related parasite populations in the western GMS.

Author summary

In the Great Mekong Subregion (GMS), particularly in Myanmar, vivax malaria remains a significant challenge to malaria elimination. To effectively evaluate the impact of ongoing malaria control measures, it is essential to understand the genetic diversity, relatedness, and population dynamics of the malaria parasite. A comprehensive analysis of *P. vivax* populations in the western GMS using a global 42-SNP barcode revealed notable changes over time. Compared to the more homogeneous parasite populations a decade ago, there has been a decrease in genetic diversity and an increase in differentiation among parasite populations in recent years, particularly along the China-Myanmar border. In comparison, the 2018 parasites from western Myanmar showed a relatively stable genetic structure, underscoring the persistent challenge of vivax malaria in this region. While the 42-SNP barcode has been valuable in understanding the genetic landscape of global *P. vivax* populations, it has limitations in accurately differentiating parasite populations across the GMS, necessitating a barcode tailored to the local parasite populations.

Introduction

Plasmodium vivax is the most widely distributed species of human malaria and is endemic in Asia, Central and South America, the Middle East, Oceania, and East Africa. In 2021, about 4.94 million malaria cases were caused by *P. vivax* worldwide, with 42% of the burden in the Southeast Asia Region [1]. Compared with *P. falciparum*, *P. vivax* is more resilient to conventional control measures due to the production of dormant hypnozoites responsible for relapses, low-density infections evading detection, and the early emergence of gametocytes favoring transmission [2,3]. Evidence that *P. vivax* can cause severe malaria and deaths continues to mount [4]. Further, *P. vivax* has become increasingly resistant to chloroquine, the first-line treatment in most vivax-endemic countries [5]. Accordingly, *P. vivax* has become the predominant malaria parasite in many endemic regions, demanding more effective strategies for its control and elimination.

Various genetic markers have been used to differentiate parasite populations, study transmission dynamics, examine epidemic events such as population decline and expansion, monitor the spread of drug-resistant parasites, and track possible infection sources and routes of introduction [6–9]. Microsatellite markers have been widely used for such analyses [10–14], and an open-access platform, VivaxGEN, has been established to standardize microsatellite-based population genetic analysis in *P. vivax* [15]. Advances in the next-generation sequencing technologies allowed whole-genome sequencing (WGS) of parasites from world populations of *P. falciparum* [16,17] and *P. vivax* [18,19], starting the new era of malaria population genomics, when parasite population structure, transmission dynamics and complexity of infection can be accurately elucidated at the whole-genome level [20, 21]. The large number of single nucleotide polymorphisms (SNPs) uncovered from the WGS of the global malaria parasite populations has enabled the selection of sets of SNP markers as “genetic barcodes” to study the parasite transmission networks and population dynamics. Compared to microsatellite panels, SNP barcodes are easier to standardize and can more accurately detect genetic diversity

between populations and geographic population structures [22]. SNP barcodes have been successfully applied to determine population transmission patterns of *P. falciparum* in different regions of the African continents [6, 23–26]. Similarly, a 42-SNP barcode was proposed for the *P. vivax* parasites based on relatively limited genome datasets [27]. A more comprehensive barcode of 71 SNPs was recently designed based on a significantly expanded *P. vivax* WGS dataset, which was shown to correctly predict the geographic origins of the parasites [28]. In addition, region-specific barcodes aiming to resolve parasite populations within a region have been designed [29,30]. More recently, a panel of 100 microhaplotypes, each containing multiple high-frequency SNPs, was designed to better resolve the global *P. vivax* populations using an amplicon-sequencing approach [31]. To date, the *P. vivax* SNP barcodes have only been used in a limited number of studies [22,27,32], while their utility in evaluating parasite population dynamics remains to be vigorously tested.

Countries of the Greater Mekong Subregion (GMS) in Southeast Asia are pursuing regional malaria elimination by 2030 [33]. Within this region, Myanmar has the highest malaria burden [34]. Like in other countries of the GMS, the proportion of malaria caused by *P. vivax* in Myanmar has increased steadily since 2012 [35,36]. As the malaria elimination course progressed, malaria transmission became concentrated along international borders and in disconnected regions. Because of the disparity of malaria incidence among regions and between the two sides of the border and extensive cross-border migration [37], it is critical to understand the genetic differences of parasite populations so that sources of imported and migration-related malaria can be traced. Studies using microsatellite markers have detected substantial geographical differentiation and temporal changes in parasite populations in the western GMS [38–40], whereas population genomics revealed a more homogeneous parasite population in the eastern GMS, Cambodia and Vietnam [30,41]. Herein, we evaluated the 42-SNP barcode to differentiate *P. vivax* populations in the western GMS, focusing on Myanmar and its adjacent areas in the Tak Province of Thailand and Yunnan Province of China.

Methods

Ethics approval

The study protocols were approved by institutional ethical committees of the collaborating institutions. Ethical approval was obtained from the institutional review boards of China Medical University, China (2019086), University of South Florida, USA (Pro00036813), Mahidol University, Thailand (TMEC11-033), and the Ministry of Health and Sports, Myanmar (Ethics/DMR/2017/077AE/2018). Written informed consent was obtained from all adult participants or the legal guardians of children before conducting the study.

Study sites and sample collection

P. vivax clinical samples were collected from patients with uncomplicated vivax malaria diagnosed by microscopy at local malaria clinics or hospitals in western China (WC2011, Yingjiang, Yunnan province, 2011, n = 58), northeast Myanmar (NEM2018, Laiza and Meomauk, 2018, n = 75), western Myanmar (WM2018, Kyauktaw and Paletwa, 2018, n = 55), and southern Myanmar (SM2011, Thanbyuzayat and Kawthaung, 2011, n = 80). Samples were also collected from bordering areas of western Thailand (WT2011, Mae Sod, Tak province, 2011, n = 47) (Fig 1). After obtaining informed consent (assent from minors), finger-prick blood was spotted on filter papers, which were dried and stored individually in plastic bags with desiccants.

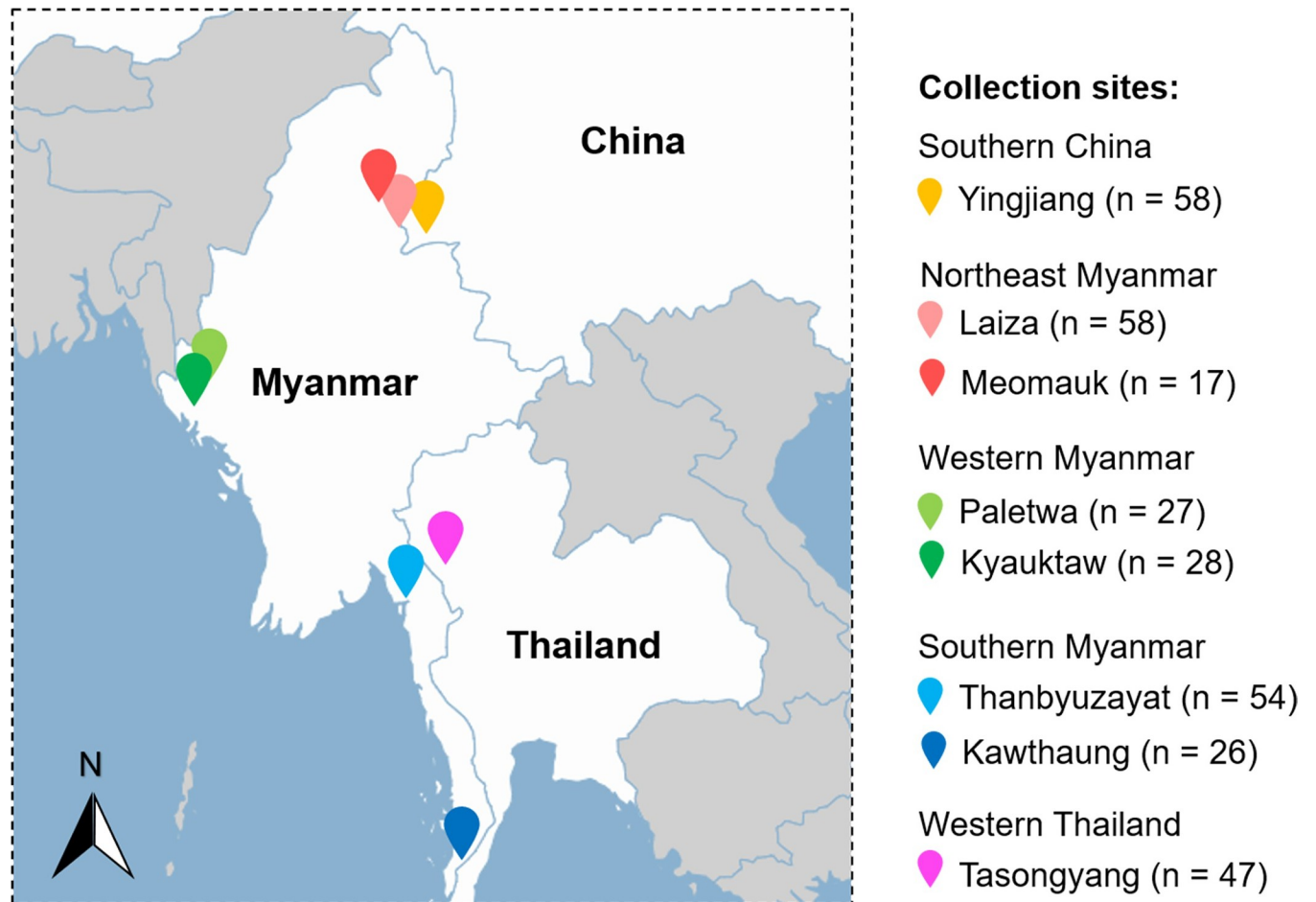


Fig 1. Map of study sample collection sites in the Great Mekong Subregion. Specific collection sites and sample sizes for SNP barcode analysis are represented by landmarks with different colors. The map was generated using the online tool available at <https://pixelmap.amcharts.com/>. The license information can be accessed at <https://www.amcharts.com/licenses/amcharts-20240401/>.

<https://doi.org/10.1371/journal.pntd.0012299.g001>

Genotyping of the 42-SNP barcode

P. vivax genomic DNA was extracted from dried blood spots on filter papers using the QIAamp DNA minikit (Qiagen). The DNA was eluted into 35–45 μ L of elution buffer and typically had an OD 260/280 of 1.6–1.8 and a concentration of > 5 ng/ μ L as measured using the NanoDrop 2000C spectrophotometer. *P. vivax* was confirmed by nested PCR targeting the *P. vivax* 18S rRNA using 2 μ L of the purified DNA [42].

The 42-SNP barcode was designed to distinguish several global *P. vivax* populations. All SNPs are bi-allelic and not located in repetitive sequences, and 18 are in protein-encoding genes [27]. High-throughput genotyping of the 42-SNP barcode was performed on the iPLEX SEQUENOM MassARRAY platform (Sequenom, CA, USA), which uses single-base extension reactions to create allele-specific products that are separated automatically and scored in a matrix-assisted laser desorption ionization/time of flight mass spectrometer. Primer design was performed using MassARRAY Assay Design software (v3.1) according to Sequenom's instructions (S1 Table). Multiplex PCR amplification of amplicons containing SNPs of interest was performed using the HotStart Taq Polymerase (Qiagen, CA, USA) with 12 ng of genomic DNA. Assay data were analyzed using Sequenom TYPER software (Typer 4.0). Genotypes of

the target sites of each sample were interpreted according to the mass spectrograph. Positive and negative controls were included in every panel to ensure genotyping accuracy. Two randomly selected *P. vivax* samples from our collection were included as positive quality control, while double-distilled water was used as negative control. Additionally, we assessed the reproducibility of genotyping by (1) subjecting the positive control samples to repeated testing in multiple panels and (2) replicating the results using the MassARRAY and Taqman platforms for samples with multiple biallelic loci. In addition, the previously published SNP barcode data for *P. vivax* samples from Africa (n = 15), South America (n = 53), and South Asia (n = 19) were downloaded for comparison [27].

Data screening and quality filtration

Only ATCG, N (mixed infection), and X (negative or missing SNP) were present in the barcode data. A sample was determined to have mixed infections if peaks matching two control genotypes were observed in at least one locus. A sample was considered negative if it showed no discernable peaks or if its peaks did not match those of any of the controls [25,43].

Minor allele frequency (MAF) was calculated from allele counts for each SNP in each population using PLINK v1.07 [44]. Because sampling was not even across all sites, we also characterized the total MAF across all populations to view regional diversity. For quality filtration, SNPs with a total MAF of less than 5% ($-maf\ 0.05$) and individuals with more than 10% missing SNP calls ($-mind\ 0.1$) were filtered out [25,43]. In addition, multiallelic SNPs with higher than 5% MAF were also considered polymorphic SNPs. For each polymorphic genotype, we counted calls for both the reference and alternate alleles by designating each with a half contribution compared to monomorphic genotypes.

Complexity of infection (COI)

Polygenomic (i.e., polyclonal) infections were established in the parasite population by examining the number of heterozygous SNPs in each sample. Since malaria parasites in the human blood are haploid, samples that carried a single allele at all positions were classified as monoclonal infections, while all other samples were considered polyclonal. Regarding samples with only one SNP site with two alleles, we followed the definition proposed by previous study and referred to them as biclonal infections [45].

The most likely number of clones in each infection was estimated with genotypes at the initially targeted SNPs using a maximum likelihood approach implemented in COIL [45,46]. The likelihood method estimated COI from the SNP genotyping data using binomial probability calculations of monomorphic vs polymorphic genotype likelihoods produced using the population MAF of the SNPs comprising the barcode panel [46]. The REAL MCCOIL method applied 10,000 iterations of Markov chain Monte Carlo (MCMC) during MAF and COI distribution estimation. It is worth mentioning that only samples with monoclonal and biclonal infection were included in the following analysis of genetic diversity and population differentiation.

Genetic diversity

To estimate within-population genetic diversity, we calculated the number of haplotypes (Nh), the number of alleles (Na), the number of effective alleles (Ae), and expected heterozygosity (He) using GenAlEx version 6.5 [47]. In addition, nucleotide diversity (π) was estimated as described [27]. To determine the distribution of genetic variance among the populations, analysis of molecular variance (AMOVA) was performed using GenAlEx version 6.5. The

correlation between geographic and genetic distances was calculated using the Mantel rank test in GenALEx version 6.5.

Effective population size (N_e)

The effective population size was calculated using the stepwise mutation model (SMM) and infinite alleles model (IAM) as previously described [48]. Mutation rates for *P. vivax* are lacking, and thus the mutation rate of *P. vivax* calibrated from an extinct European strain (5.57×10^{-7} , 95% CI: 2.75×10^{-8} – 1.06×10^{-6}) was used [49].

Genetic differentiation and population structure analysis

Based on quality-controlled data, we calculated the pairwise F_{ST} [50] in five populations using VCFtools [51]. Genetic differentiation was divided into three levels according to the F_{ST} value: low (≤ 0.15), moderate (0.15–0.25), and high (≥ 0.25) [52].

Principal component analysis (PCA) was performed by constructing a genetic relationship matrix and estimating eigenvalues and eigenvectors for the principal components using PLINK 1.07 [53]. A two-dimensional scatter plot of the first two principal components was drawn using R (www.rproject.org/). In addition, phylogenetic relationships amongst *P. vivax* isolates were analyzed using the Neighbour-Joining method [54] implemented in MEGA7 [55]. The genetic structure of the five populations was analyzed with ADMIXTURE [56]. Ten runs were performed, with K values ranging from 1 to 10, and the one with the lowest cross-validation error was selected.

Results

Genotyping the 42-SNP barcode

We genotyped 315 samples for the 42-SNP barcode in two panels on the MassARRAY platform. To assist SNP calling and ensure accuracy, we included two positive and two negative controls. The peaks corresponding to the reference or alternative bases were consistent in the positive control samples but were either undetected or appeared as minor peaks in negative controls (S1 Fig). The overall genotyping success rate was 97.4% ($\geq 94.0\%$ at individual loci) (S1 Data). Based on the filtering criteria, SNPs at positions 530130 on chromosome (chr) 2, 828771 on chr 13, and 427515 on chr 14 with total MAF value below 0.05 were filtered out, leaving 39 SNPs for analysis (S2 Table). Thirty-six SNPs had total MAF above 0.1 (Fig 2 and S2 Table), while SNPs at positions 668364 on chr 1, 705724 on chr 11, and 1108185 on chr 12 had relatively low diversity with total MAF of 0.056, 0.093, and 0.097, respectively (S2 Table). Each sampling site had 35–37 SNPs with MAFs greater than 0.1 (S2 Fig). For SNPs with an MAF greater than 0.3, the WM2018 population had 23 SNPs, and the NEM2018 population had only 15 SNPs (S2 Fig). Meanwhile, 24 samples with more than 10% missing SNP calls (—mind 0.1) were excluded from the analysis. A total of 291 samples were successfully genotyped at 39 SNPs, with only 34 infections (11.7%) exhibiting monoallelicity at each nucleotide position (i.e., monoclonal), while the remaining 257 (88.3%) samples displayed two alleles with ≥ 1 SNP (i.e., polyclonal). Among the latter, 100 infections (38.9%) showed two alleles at a single locus (i.e., biclonal). Ultimately, 134 samples (23 from WC2011, 49 from NEM2018, 14 from WM2018, 25 from SM2011, and 23 from WT2011) with monoclonal and biclonal infections were used for population genetic analyses (S3 Table). The analysis utilized a total of 234 SNP-sequences, with the inclusion of 200 SNP-sequences derived from the generation of 100 biclonal samples.

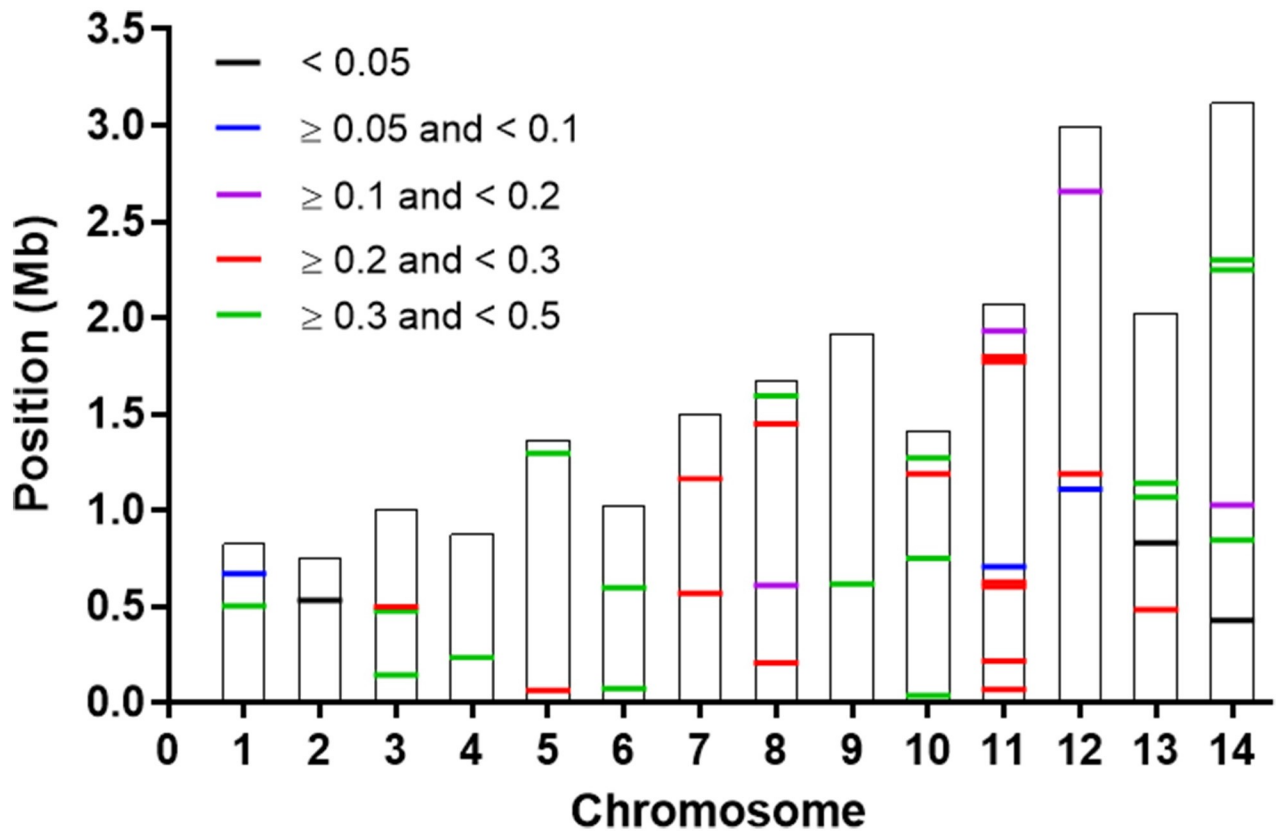


Fig 2. The total minor allele frequency (MAF) of 42 SNPs. The location of the 42 SNPs is illustrated on the 14 chromosomes of the *P. vivax* genome. SNPs were colored by total MAF. 17 SNPs had $0.3 \leq \text{MAF} < 0.5$, 15 SNPs had $0.2 \leq \text{MAF} < 0.3$, 4 SNPs had $0.1 \leq \text{MAF} < 0.2$, 3 SNPs had $0.05 \leq \text{MAF} < 0.1$, 3 SNPs had $\text{MAF} < 0.05$.

<https://doi.org/10.1371/journal.pntd.0012299.g002>

Complexity of infection (COI)

Genotyping results at the 39 SNPs showed that 88.3% of the *P. vivax* samples were polyclonal infections. The proportions of polyclonal infections differed significantly among the five *P. vivax* populations ($P = 0.0012$, Pearson Chi-square test, $\chi^2 = 18.1$), highest (96.2.1%, 50/52) in the 2018 western Myanmar (WM) population and lowest (77.1%, 54/70) in the 2018 northeast Myanmar (NEM) population (WM vs NEM in 2018: $P = 0.004$, Fisher's exact test) (Fig 3A). Samples collected in 2011 in southern Myanmar had a significantly higher proportion of polyclonal infections than in other two regions ($P = 0.031$, Pearson Chi-square test, $\chi^2 = 6.9$). Likewise, the average COI was also highest in WM (1.31) and lowest in NEM (1.01) in 2018 (Fig 3B). In the GMS, we did not observe a significant association between the proportion of polyclonal infections or the most likely number of clones and the year of collection ($P = 0.196$, Fisher's exact test; $P = 0.950$, Student's t-test). However, we noticed that both values were slightly higher in the samples collected during the early years. In more recent years, a similar COI has been discovered along the China-Myanmar border, as well as in previous years. Although the polyclonal proportion was higher in the early years compared to recent years (90.74% vs. 77.14%), the difference was not statistically significant ($P = 0.055$, Fisher's exact test).

Population diversity

The pairwise nucleotide diversity (π), number of haplotypes (Nh), number of different alleles (Na), number of effective alleles (Ae), and expected heterozygosity (He) for each population

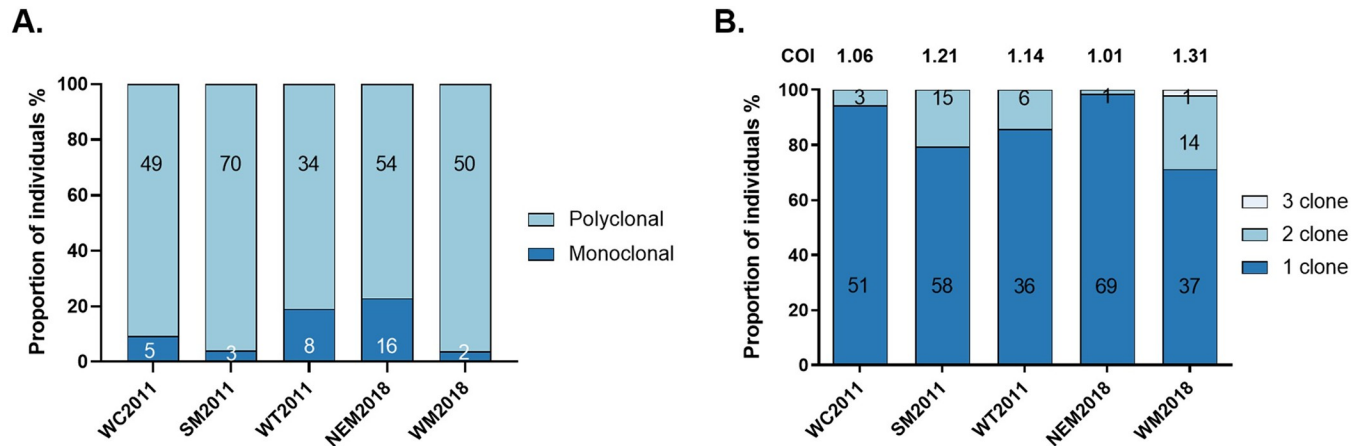


Fig 3. Complexity of infection in different *P. vivax* populations in the GMS. (A) Monoclonal and polyclonal infections were calculated using genotypes at the initially targeted SNPs, with samples carrying a single allele at all positions being classified as monoclonal infections. (B) The most likely number of clones was estimated using the COIL web-based tool. Numbers within the bars indicate the sampling size for each category. The estimated numbers of polyclonal/monoclonal samples differ between the two methods.

<https://doi.org/10.1371/journal.pntd.0012299.g003>

are shown in Table 1. Of these, the π value of WM was significantly higher than that of NEM2018 ($P < 0.0001$, Student’s t-test). For the sites along the eastern Myanmar border, π values of samples collected in 2011 varied slightly, ranging from 0.348 to 0.388, which were significantly higher than that in the NEM2018 parasites ($P < 0.0001$, Student’s t-test). At the China-Myanmar border, nucleotide diversity in parasite populations showed a noticeable reduction from 0.388 in 2011 (WC2011) to 0.224 in 2018 (NEM2018) ($P < 0.0001$, Student’s t-test). Remarkably, 100 (74.62%) unique haplotypes were detected in these 134 samples with mono-clonal and biconal infections (Table 1). Likewise, the WC, SM, and WT parasite populations harbored the greatest number of haplotypes in 2011. A pronounced decrease in the expected heterozygosity was observed at the China-Myanmar border from 0.363 in 2011 to 0.22 in 2018 ($P < 0.0001$, Student’s t test) (Table 1). Collectively, the *P. vivax* populations from the western GMS in 2011 were highly diverse without statistically significant differences among sites, while the diversity showed considerable reductions in recent years (2018).

We used the SMM and IAM models to estimate the effective population size (N_e) of *P. vivax* populations in the GMS. When the new *P. vivax* mutation rate was used, the N_e was largest in WC2011, followed by WM2018, and the smallest N_e was found in NEM2018 (Table 2), consistent with the results of nucleotide diversity.

Table 1. Genetic diversity of *P. vivax* populations in the GMS.

Population	N	$\pi \pm SD$	Nh	$Na \pm SE$	$Ae \pm SE$	$He \pm SE$
WC2011	23	0.388 ± 0.046	23	2.000 ± 0.000	1.624 ± 0.046	0.363 ± 0.020
SM2011	25	0.378 ± 0.044	24	1.949 ± 0.036	1.593 ± 0.041	0.354 ± 0.020
WT2011	23	0.348 ± 0.043	23	1.923 ± 0.057	1.577 ± 0.056	0.331 ± 0.026
NEM2018	49	0.224 ± 0.036	20	1.923 ± 0.043	1.347 ± 0.033	0.220 ± 0.026
WM2018	14	0.384 ± 0.050	10	1.897 ± 0.049	1.615 ± 0.050	0.352 ± 0.025
Total	134	0.363 ± 0.034	100	2.000 ± 0.000	1.616 ± 0.042	0.364 ± 0.018

N, number of samples; π , pairwise nucleotide diversity; Nh , number of haplotypes; Na , number of different alleles; Ae , number of effective alleles; He , expected heterozygosity; SD, standard deviation; SE, standard error. WC, western China; NEM, northeastern Myanmar; WM, western Myanmar; SM, southern Myanmar; WT, western Thailand.

<https://doi.org/10.1371/journal.pntd.0012299.t001>

Table 2. Effective population size (N_e) of the *P. vivax* populations was estimated using the SMM and IAM models.

Populations	SMM	95%CI	IAM	95%CI
WC2011	328648	172695–6656620	255771	134401–5180534
SM2011	313345	164654–6346662	245955	129242–4981706
WT2011	248317	130484–5029547	202594	106457–4103444
NEM2018	144447	75903–2925707	126594	66522–2564103
WM2018	310031	162912–6279531	243811	128116–4938272
Total	330389	173610–6691874	256879	134982–5202973

Mutation rate (μ) of *P. vivax* of 5.57×10^{-7} (95% confidence interval: 2.75×10^{-8} , 1.06×10^{-6}) was used. SMM, stepwise mutational model; IAM, infinite allele model. WC, western China; NEM, northeastern Myanmar; WM, western Myanmar; SM, southern Myanmar; WT, western Thailand.

<https://doi.org/10.1371/journal.pntd.0012299.t002>

Genetic variation and differentiation

AMOVA analysis revealed that the majority of the variations (87%) in *P. vivax* was found within populations in the GMS rather than between populations (S3 Fig). Mantel testing was conducted to determine the correlation between pairwise genetic and geographic distances of *P. vivax* populations, which showed a correlation coefficient $r^2 = 0.1693$ ($P = 0.140$) (S4 Fig). To further clarify if genetic differentiation of the *P. vivax* populations existed in the GMS, Wright's fixation index F_{ST} was estimated between each pair of the populations (Fig 4). Pairwise comparison determined the F_{ST} values ranging from 0.003 to 0.252. It is noteworthy that the NEM2018 parasite populations had moderate to high genetic differentiation from all other populations, with an F_{ST} value ranging from 0.162 to 0.252 (Fig 4). In particular, although the NEM2018 and WC2011 were essentially from the same area, the two longitudinal populations still had moderate genetic differentiation ($F_{ST} = 0.165$). In 2018, *P. vivax* from NEM and WM showed the highest genetic differentiation ($F_{ST} = 0.252$). In contrast, the other six pairwise comparisons did not show much genetic differentiation, with F_{ST} less than 0.15 (Fig 4). A global genetic differentiation analysis comparing *P. vivax* populations from the GMS, South America, Africa, and South Asia showed F_{ST} values ranging from 0.231 to 0.419 (S4 Table), which supports substantial division of the global *P. vivax* populations.

Population structure

We further compared the *P. vivax* populations from different regions using PCA, phylogeny, and ADMIXTURE analysis. The PCA analysis revealed that the 39-SNP barcode sufficiently differentiated the global populations (S5A Fig), indicating that the removal of three SNPs (total MAF < 0.05) did not affect the overall effectiveness of the 42-SNP barcode. The main cluster comprised parasites from the GMS, which were separated from populations in Africa, South Asia, and South America (S5B Fig). We then used the 39-SNP barcode to perform PCA on *P. vivax* populations within the GMS. The results showed that the top two principal components accounted for 68.67% (PC1) and 31.33% (PC2) of the total variability. The NEM2018 population formed several clusters, and two clusters were well separated from other *P. vivax* populations from the GMS (Fig 5A). However, the rest of the populations, consisting of samples collected in 2011 and from western Myanmar in 2018, could not be confidently separated, suggesting close genetic relationships.

Phylogenetic analysis used to infer the genetic relationships among populations in the GMS identified four large clusters of parasites in the neighbor-joining tree (Fig 5B). Although each cluster contained parasites from all four sample collections, Cluster 4 included most of the NEM2018 samples. In particular, the NEM2018 samples in Cluster 4 formed a distinct clade, which contained three closely related main subclades. In a global analysis, the GMS population

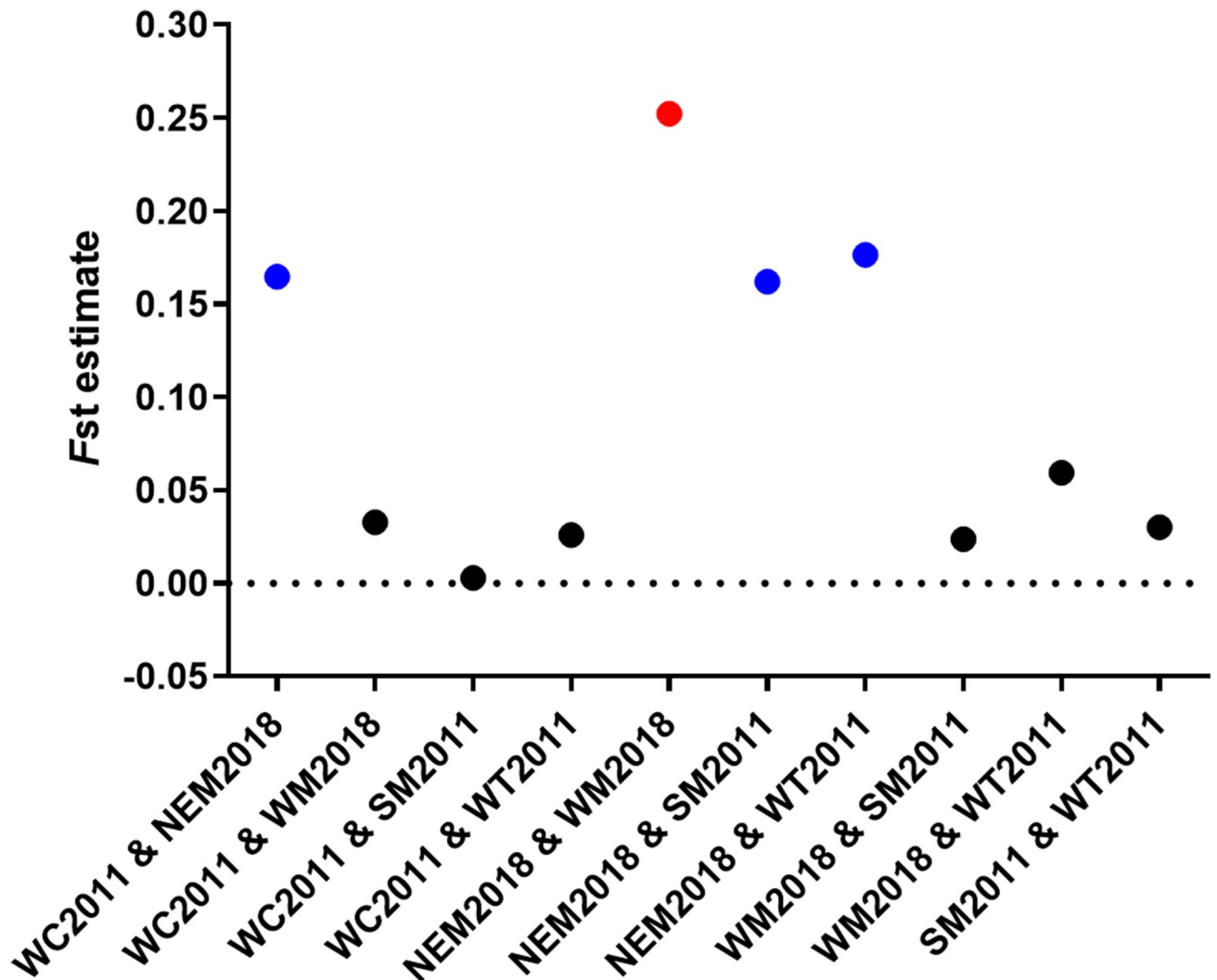


Fig 4. Pairwise comparison of F_{ST} among *P. vivax* populations in the GMS. Red, blue and black points represent high ($F_{ST} \geq 0.25$), moderate ($0.15 < F_{ST} < 0.25$), and low genetic differentiation ($F_{ST} \leq 0.15$), respectively.

<https://doi.org/10.1371/journal.pntd.0012299.g004>

was also clearly distinguished from other populations from South Asia, Africa, and South America (S6 Fig).

The ADMIXTURE analysis of the western GMS samples revealed the presence of multiple subpopulations. Using the 39 SNPs with MAF above 0.05, we found that the lowest cross-validation error was at $K = 2$, which is considered the optimal number of populations (S7 Fig). At $K = 2$, all five parasite populations from GMS had admixed haplotypes and clustered into blue and red sub-populations (Fig 5C). The genetic structure patterns of four parasite populations, WC2011, SM2011, WT2011, and WM2018, were very similar, suggesting that many of these parasites had shared ancestry. In contrast, the NEM2018 population was genetically distinctive, with the blue sub-population dominated, which may reflect a process of population replacement.

Discussion

The 42-SNP barcode with SNPs spanning all 14 chromosomes of the *P. vivax* genome was able to differentiate *P. vivax* populations among South Asia, Africa, and South America [27]. We

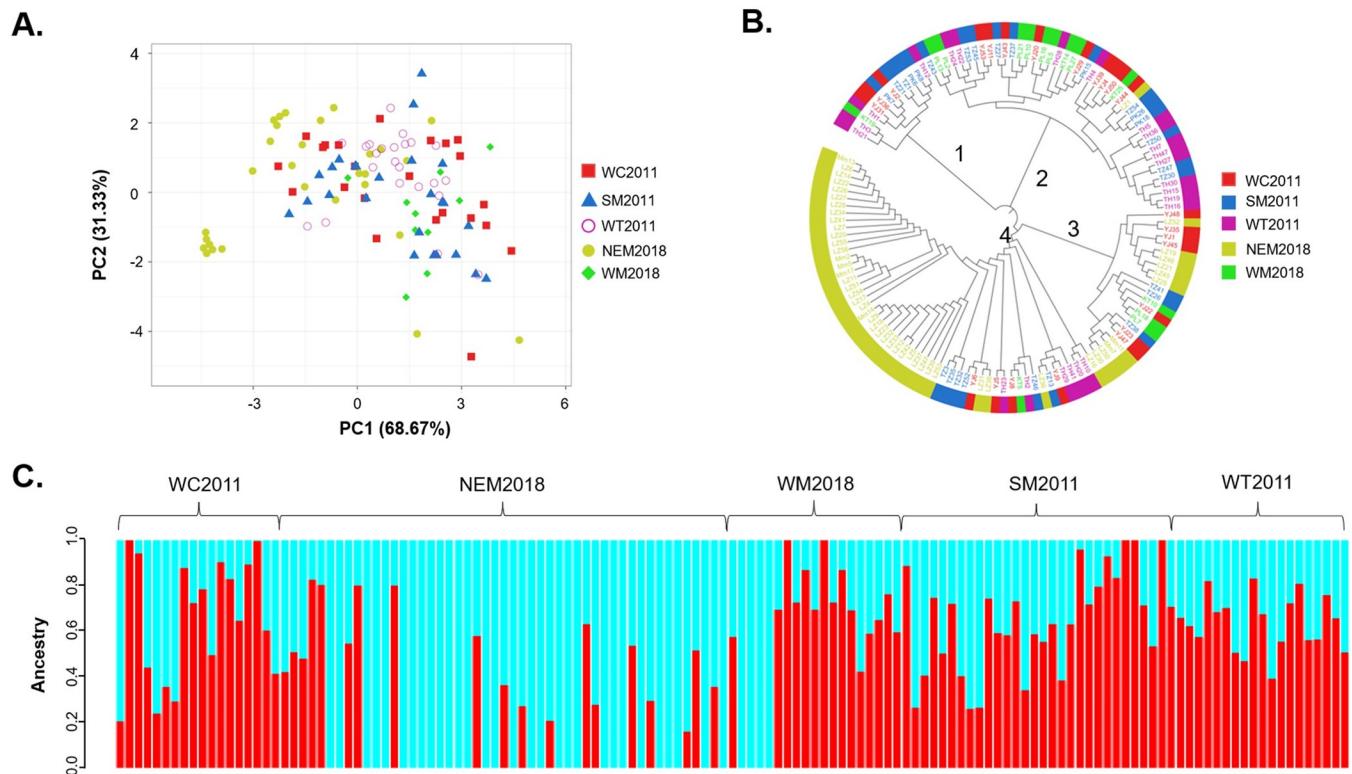


Fig 5. Clustering patterns of *P. vivax* isolates collected from the GMS. (A) Principal component analysis of the GMS samples. (B) Phylogenetic analysis of *P. vivax* isolates based on neighbor-joining method. (C) ADMIXTURE analysis for $K = 2$. Vertical bars indicate individual *P. vivax* haplotypes, and colors represent individual assignments to inferred clusters.

<https://doi.org/10.1371/journal.pntd.0012299.g005>

utilized the Agena Bioscience MassARRAY System, a cost-effective and high-throughput platform that is compatible with the multiplex PCR design [57], to genotype 315 *P. vivax* parasite isolates collected from the western GMS using the 42 SNPs, with a 92% success rate. Failed samples were likely due to low DNA concentrations extracted from single blood spots on filter paper. This study extended the usability of the 42-SNP barcode to differentiate *P. vivax* populations from different continents, including Southeast Asia, despite removing three SNPs with MAF less than 0.05, which further validates the 42-SNP barcode as an effective way to track parasite origins to continents.

The COI provides valuable insights into disease transmission and epidemiology. Many methods estimate COI based on PCR amplification of one or more genetic loci with insertion/deletion polymorphisms, such as the *P. vivax* merozoite surface protein genes (*pvmsp3α* and *pvmsp3β*) and circumsporozoite protein [58–62]. In comparison, genotyping multiple loci is more accurate for detecting multiclinal infections. Our analysis revealed an average of 88.3% polyclonal *P. vivax* infections in the western GMS, comparable to the eastern GMS (e.g., 92% in Cambodia based on the analysis of a 100-SNP barcode) [45]. In this regard, the proportion of polyclonal infections in *P. vivax* samples in the GMS are much higher than in South Asia (41.2–79.0%), South America (52.8%), and Africa (39–60%) [27,32,63]. In contrast, analysis of similar *P. vivax* populations in the GMS by genotyping microsatellites only detected 14.6–30.7% as multiclinal infections [39, 40], further supporting the increasing power of the SNP barcode in detecting mixed infections. Within the western GMS, *P. vivax* samples from western Myanmar showed significantly higher COI than in northeastern Myanmar, reflecting

higher *P. vivax* transmission intensity in western Myanmar, as we previously noted [64]. A notable observation from the analysis of longitudinal samples from northeast Myanmar is the significantly increased proportions of monoclonal infections from 2011 to 2018, which may reflect the more extensive control efforts delivered to this region. The northeast Myanmar site bordering China's Yunnan Province is located in an extended buffer zone, where Yunnan's malaria control program has implemented intensive malaria control efforts under its "3 + 1" strategy [65,66].

The *P. vivax* populations in the western GMS displayed moderate to high levels of genetic diversity, with the π values ranging from 0.224 to 0.388. Previous studies of GMS *P. vivax* populations using microsatellite markers identified H_e values of 0.66–0.86 [40,67,68], much higher than we found in this study (0.22–0.36). This difference may be related to the different genotyping methods used. Nevertheless, the effective population size N_e at the China-Myanmar border showed a ~ twofold decrease over seven years, consistent with the decreased genetic diversity of the parasite population. In comparison, the genetic diversity in the 2018 western Myanmar population was comparable to that in other regions of Myanmar in 2011, suggesting that control efforts did not significantly reduce parasite populations in the western border of Myanmar. Notably, one limitation of the study is that the China-Myanmar border samples were collected from two sites located on different sides of the border, although they are adjacent and connected by a major port facilitating migration.

F-statistics and population structure analysis suggested a relatively panmictic *P. vivax* population in the western GMS in 2011 before regional malaria elimination was on the agenda [33]. The higher within-population than between-population genetic variances also support this conclusion. However, parasites collected in 2018 from the China-Myanmar border formed distinct clades or clusters, suggesting increasing differentiation of *P. vivax* populations in the GMS in recent years. This is consistent with the population genomics analysis of *P. vivax* samples collected from northeast Myanmar, which were genetically distinct from other parts of the GMS [30]. Within the clusters, there were many closely related parasites suggesting results of clonal expansion. Such speculation is consistent with the *P. vivax* epidemiology in northeast Myanmar, where a vivax malaria outbreak occurred in 2016 [35]. The *P. vivax* population structure and dynamics in northeast Myanmar exhibited initial contraction of the parasite population and subsequent rapid clonal expansion, akin to the parasite population dynamics observed during the malaria pre-elimination phase in Malaysia [69].

Analyses of global *P. vivax* populations using microsatellites, antigens, and genome-wide SNPs have all identified strong geographic population structures between continents [12,18,19,70]. Similarly, the 42-SNP barcode captured differences between *P. vivax* populations from Africa, South America, South Asia, and Southeast Asia, but its ability to differentiate local populations within the GMS is limited. There are several possible explanations. Firstly, differences in selective pressure (human hosts, mosquito vectors, ecological environment, and malaria control measures) are strong at the global level but weak at the local level, resulting in less differentiated local parasite populations. The primary vectors *An. dirus* and *An. minimus* are widely distributed across the GMS [34]. As the GMS is pursuing regional malaria elimination, major malaria control measures, such as long-lasting insecticide-treated bed nets and indoor residual spraying, have been extensively deployed, and chloroquine/primaquine remains the frontline treatment for *P. vivax* malaria [34]. Thus, these factors may not have imposed strong region-specific selection on *P. vivax* population in the GMS. Secondly, parasite populations in the GMS were more or less panmictic due to the large effective population sizes, geographic connectivity, and considerable mixing resulting from extensive human migration [7,71]. Economic development in the GMS has facilitated large-scale human mobility, including cross-border labor migration, enabling transnational malaria introduction and

parasite population mixing [72, 73]. Thirdly, the 42 SNP alleles in the barcode were not informative for the GMS parasite populations, as they were selected based on F_{ST} values among global populations. Accordingly, after analyzing the *P. vivax* genomes from different regions of the GMS, another panel of SNPs was selected as local markers to differentiate parasite populations within this region [30], which awaits future validation.

Conclusion

Despite notable progress in malaria prevention and control, vivax malaria continues to present a significant challenge in the GMS region, particularly in Myanmar. To assess the effectiveness of ongoing malaria control efforts, it is crucial to have a genotyping tool that can offer insights into the genetic diversity, relatedness, and transmission patterns of vivax malaria populations. Analysis of *P. vivax* populations in the western GMS using a global 42-SNP barcode found more homogeneous parasite populations a decade ago but a less diverse and more differentiated parasite population from the China-Myanmar border in recent years. However, the 2018 western Myanmar parasite population did not show substantial changes in genetic diversity and population structure, stressing the need for strengthened malaria control efforts in this region. Notably, although the chronological changes observed in the different sites were consistent with the changes in malaria transmission intensity, we cannot exclude potential influences of sample collection bias since all samples were convenience samples from acute vivax patients. The 42-SNP barcode has limitations in differentiating *P. vivax* populations across the GMS, requiring an extended barcode tailored to local parasite populations.

Supporting information

S1 Fig. Mass spectrometry peaks of quality control samples were detected by using Typer 4.0 software.

(TIF)

S2 Fig. The minor allele frequency of 42 SNPs per sub-region.

(TIF)

S3 Fig. Analysis of molecular variance of *P. vivax* isolates obtained from the GMS.

(TIF)

S4 Fig. Mantel test of *P. vivax* isolates obtained from the GMS.

(TIF)

S5 Fig. Principal coordinate analysis of the global sample sites. (A) The lessened barcode of 39 SNPs showed same ability to distinguish *P. vivax* populations as 42-SNP barcode. (B) Parasites from the GMS made up the main cluster, separated from Africa, south Asia and South America populations.

(TIF)

S6 Fig. The phylogenetic analysis of the global sample sites.

(TIF)

S7 Fig. K-value (K = 2) had the lowest cross validation error (CV-error).

(TIF)

S1 Table. 42-SNP molecular barcode and primers.

(DOCX)

S2 Table. Minor allele frequency (MAF) of *P. vivax* populations. Red font indicates that the total MAF value is less than 0.05. WC, western China; NEM, northeastern Myanmar; WM, western Myanmar; SM, southern Myanmar; WT, western Thailand.

(DOCX)

S3 Table. Clinical *P. vivax* samples were included in this study.

(DOCX)

S4 Table. Pairwise comparison of F_{ST} among global *P. vivax* populations.

(DOCX)

S1 Dataset. Barcodes for the 315 clinical *P. vivax* isolates in the GMS. The top panel shows the assays number its corresponding reference (REF.) or alternate allele (ALT.) and chromosome (Chrom.) position. The reference allele is shown in white, the alternate allele in gray, polygenomic genotypes with both alleles are labeled N and is shown in blue, missing SNPs are labeled X and is shown in red.

(XLSX)

Acknowledgments

We want to thank the medical staff at the clinics for collecting the parasite samples and the patients for providing blood samples for this study.

Author Contributions

Conceptualization: Yubing Hu, Liwang Cui, Yaming Cao.

Data curation: Yubing Hu, Yuling Li, Awtum M. Brashear, Weilin Zeng, Zifang Wu, Yan Zhao.

Formal analysis: Yuling Li, Awtum M. Brashear, Weilin Zeng, Zifang Wu, Yan Zhao.

Funding acquisition: Liwang Cui.

Investigation: Lin Wang, Haichao Wei, Myat Thu Soe, Pyae Linn Aung, Jetsumon Sattabongkot, Myat Phone Kyaw, Zhaoqing Yang, Yan Zhao.

Methodology: Yubing Hu, Yuling Li, Lin Wang, Haichao Wei, Yan Zhao.

Project administration: Liwang Cui, Yaming Cao.

Resources: Myat Thu Soe, Pyae Linn Aung, Jetsumon Sattabongkot, Myat Phone Kyaw, Zhaoqing Yang.

Supervision: Jetsumon Sattabongkot, Myat Phone Kyaw, Zhaoqing Yang, Liwang Cui.

Visualization: Yuling Li, Awtum M. Brashear, Weilin Zeng, Zifang Wu, Yan Zhao.

Writing – original draft: Yubing Hu, Yuling Li, Yan Zhao, Liwang Cui, Yaming Cao.

Writing – review & editing: Yan Zhao, Liwang Cui, Yaming Cao.

References

1. WHO. World Malaria Report 2023. Geneva: World Health Organization. 2023. <https://doi.org/teams/global-malaria-programme/reports/world-malaria-report-2020>
2. Adams JH, Mueller I. The biology of *Plasmodium vivax*. Cold Spring Harb Perspect Med. 2017; 7(9): a025585. Epub 2017/05/12. <https://doi.org/10.1101/cshperspect.a025585> PMID: 28490540.

3. Cui L, Brashear A, Menezes L, Adams J. Elimination of *Plasmodium vivax* malaria: problems and solutions. *Current Topics and Emerging Issues in Malaria Elimination*: IntechOpen; 2021. p. 27.
4. Naing C, Whittaker MA, Nyunt Wai V, Mak JW. Is *Plasmodium vivax* malaria a severe malaria?: a systematic review and meta-analysis. *PLoS Negl Trop Dis*. 2014; 8(8):e3071. Epub 2014/08/15. <https://doi.org/10.1371/journal.pntd.0003071> PMID: 25121491.
5. Price RN, von Seidlein L, Valecha N, Nosten F, Baird JK, White NJ. Global extent of chloroquine-resistant *Plasmodium vivax*: a systematic review and meta-analysis. *Lancet Infect Dis*. 2014; 14(10):982–91. Epub 2014/09/13. [https://doi.org/10.1016/S1473-3099\(14\)70855-2](https://doi.org/10.1016/S1473-3099(14)70855-2) PMID: 25213732.
6. Daniels RF, Schaffner SF, Wenger EA, Proctor JL, Chang HH, Wong W, et al. Modeling malaria genomics reveals transmission decline and rebound in Senegal. *Proc Natl Acad Sci U S A*. 2015; 112(22):7067–72. Epub 2015/05/06. <https://doi.org/10.1073/pnas.1505691112> PMID: 25941365.
7. Barry AE, Waltmann A, Koepfli C, Barnadas C, Mueller I. Uncovering the transmission dynamics of *Plasmodium vivax* using population genetics. *Pathog Glob Health*. 2015; 109(3):142–52. Epub 2015/04/22. <https://doi.org/10.1179/2047773215Y.0000000012> PMID: 25891915.
8. Auburn S, Barry AE. Dissecting malaria biology and epidemiology using population genetics and genomics. *Int J Parasitol*. 2017; 47(2–3):77–85. Epub 2016/11/09. <https://doi.org/10.1016/j.ijpara.2016.08.006> PMID: 27825828.
9. Shetty AC, Jacob CG, Huang F, Li Y, Agrawal S, Saunders DL, et al. Genomic structure and diversity of *Plasmodium falciparum* in Southeast Asia reveal recent parasite migration patterns. *Nat Commun*. 2019; 10(1):2665. Epub 2019/06/19. <https://doi.org/10.1038/s41467-019-10121-3> PMID: 31209259.
10. Ferreira MU, Karunaweera ND, da Silva-Nunes M, da Silva NS, Wirth DF, Hartl DL. Population structure and transmission dynamics of *Plasmodium vivax* in rural Amazonia. *J Infect Dis*. 2007; 195(8):1218–26. Epub 2007/03/16. <https://doi.org/10.1086/512685> PMID: 17357061.
11. Gunawardena S, Ferreira MU, Kapilananda GM, Wirth DF, Karunaweera ND. The Sri Lankan paradox: high genetic diversity in *Plasmodium vivax* populations despite decreasing levels of malaria transmission. *Parasitology*. 2014; 141(7):880–90. Epub 2014/02/19. <https://doi.org/10.1017/S0031182013002278> PMID: 24533989.
12. Koepfli C, Rodrigues PT, Antao T, Orjuela-Sanchez P, Van den Eede P, Gamboa D, et al. *Plasmodium vivax* Diversity and Population Structure across Four Continents. *PLoS Negl Trop Dis*. 2015; 9(6):e0003872. Epub 2015/07/01. <https://doi.org/10.1371/journal.pntd.0003872> PMID: 26125189.
13. Kattenberg JH, Razook Z, Keo R, Koepfli C, Jennison C, Lautu-Gumal D, et al. Monitoring *Plasmodium falciparum* and *Plasmodium vivax* using microsatellite markers indicates limited changes in population structure after substantial transmission decline in Papua New Guinea. *Mol Ecol*. 2020; 29(23):4525–41. Epub 2020/09/29. <https://doi.org/10.1111/mec.15654> PMID: 32985031.
14. Rougeron V, Elguero E, Arnathau C, Acuna Hidalgo B, Durand P, Houze S, et al. Human *Plasmodium vivax* diversity, population structure and evolutionary origin. *PLoS Negl Trop Dis*. 2020; 14(3):e0008072. Epub 2020/03/10. <https://doi.org/10.1371/journal.pntd.0008072> PMID: 32150544.
15. Trimarsanto H, Benavente ED, Noviyanti R, Utami RA, Trianty L, Pava Z, et al. VivaxGEN: An open access platform for comparative analysis of short tandem repeat genotyping data in *Plasmodium vivax* populations. *PLoS Negl Trop Dis*. 2017; 11(3):e0005465. Epub 2017/04/01. <https://doi.org/10.1371/journal.pntd.0005465> PMID: 28362818.
16. Miotto O, Almagro-Garcia J, Manske M, Macinnis B, Campino S, Rockett KA, et al. Multiple populations of artemisinin-resistant *Plasmodium falciparum* in Cambodia. *Nat Genet*. 2013; 45(6):648–55. Epub 2013/04/30. <https://doi.org/10.1038/ng.2624> PMID: 23624527.
17. Amambua-Ngwa A, Amenga-Etego L, Kamau E, Amato R, Ghansah A, Golassa L, et al. Major subpopulations of *Plasmodium falciparum* in sub-Saharan Africa. *Science*. 2019; 365(6455):813–6. Epub 2019/08/24. <https://doi.org/10.1126/science.aav5427> PMID: 31439796.
18. Hupalo DN, Luo Z, Melnikov A, Sutton PL, Rogov P, Escalante A, et al. Population genomics studies identify signatures of global dispersal and drug resistance in *Plasmodium vivax*. *Nat Genet*. 2016; 48(8):953–8. Epub 2016/06/28. <https://doi.org/10.1038/ng.3588> PMID: 27348298.
19. Pearson RD, Amato R, Auburn S, Miotto O, Almagro-Garcia J, Amaratunga C, et al. Genomic analysis of local variation and recent evolution in *Plasmodium vivax*. *Nat Genet*. 2016; 48(8):959–64. Epub 2016/06/28. <https://doi.org/10.1038/ng.3599> PMID: 27348299.
20. Neafsey DE, Taylor AR, MacInnis BL. Advances and opportunities in malaria population genomics. *Nat Rev Genet*. 2021; 22(8):502–17. Epub 2021/04/10. <https://doi.org/10.1038/s41576-021-00349-5> PMID: 33833443.
21. Brashear AM, Cui L. Population genomics in neglected malaria parasites. *Front Microbiol*. 2022; 13:984394. Epub 2022/09/27. <https://doi.org/10.3389/fmicb.2022.984394> PMID: 36160257.

22. Fola AA, Kattenberg E, Razook Z, Lautu-Gumal D, Lee S, Mehra S, et al. SNP barcodes provide higher resolution than microsatellite markers to measure *Plasmodium vivax* population genetics. *Malar J*. 2020; 19(1):375. Epub 2020/10/22. <https://doi.org/10.1186/s12936-020-03440-0> PMID: 33081815.
23. Mharakurwa S, Daniels R, Scott A, Wirth DF, Thuma P, Volkman SK. Pre-amplification methods for tracking low-grade *Plasmodium falciparum* populations during scaled-up interventions in Southern Zambia. *Malar J*. 2014; 13:89. Epub 2014/03/13. <https://doi.org/10.1186/1475-2875-13-89> PMID: 24618119.
24. Sisyá TJ, Kamn'gona RM, Vareta JA, Fulakeza JM, Mukaka MF, Seydel KB, et al. Subtle changes in *Plasmodium falciparum* infection complexity following enhanced intervention in Malawi. *Acta Trop*. 2015; 142:108–14. Epub 2014/12/03. <https://doi.org/10.1016/j.actatropica.2014.11.008> PMID: 25460345.
25. Bankole BE, Kayode AT, Nosamiefan IO, Eromon P, Baniecki ML, Daniels RF, et al. Characterization of *Plasmodium falciparum* structure in Nigeria with malaria SNPs barcode. *Malar J*. 2018; 17(1):472. Epub 2018/12/19. <https://doi.org/10.1186/s12936-018-2623-8> PMID: 30558627.
26. Amambua-Ngwa A, Jeffries D, Mwesigwa J, Seedy-Jawara A, Okebe J, Achan J, et al. Long-distance transmission patterns modelled from SNP barcodes of *Plasmodium falciparum* infections in The Gambia. *Sci Rep*. 2019; 9(1):13515. Epub 2019/09/20. <https://doi.org/10.1038/s41598-019-49991-4> PMID: 31534181.
27. Baniecki ML, Faust AL, Schaffner SF, Park DJ, Galinsky K, Daniels RF, et al. Development of a single nucleotide polymorphism barcode to genotype *Plasmodium vivax* infections. *PLoS Negl Trop Dis*. 2015; 9(3):e0003539. Epub 2015/03/18. <https://doi.org/10.1371/journal.pntd.0003539> PMID: 25781890.
28. Diez Benavente E, Campos M, Phelan J, Nolder D, Dombrowski JG, Marinho CRF, et al. A molecular barcode to inform the geographical origin and transmission dynamics of *Plasmodium vivax* malaria. *PLoS Genet*. 2020; 16(2):e1008576. Epub 2020/02/14. <https://doi.org/10.1371/journal.pgen.1008576> PMID: 32053607.
29. de Oliveira TC, Rodrigues PT, Menezes MJ, Goncalves-Lopes RM, Bastos MS, Lima NF, et al. Genome-wide diversity and differentiation in New World populations of the human malaria parasite *Plasmodium vivax*. *PLoS Negl Trop Dis*. 2017; 11(7):e0005824. Epub 2017/08/02. <https://doi.org/10.1371/journal.pntd.0005824> PMID: 28759591.
30. Brashear AM, Fan Q, Hu Y, Li Y, Zhao Y, Wang Z, et al. Population genomics identifies a distinct *Plasmodium vivax* population on the China-Myanmar border of Southeast Asia. *PLoS Negl Trop Dis*. 2020; 14(8):e0008506. Epub 2020/08/04. <https://doi.org/10.1371/journal.pntd.0008506> PMID: 32745103.
31. Siegel SV, Amato R, Trimarsanto H, Sutanto E, Kleinecke M, Murie K, et al. Lineage-informative micro-haplotypes for spatio-temporal surveillance of *Plasmodium vivax* malaria parasites. *medRxiv*. 2023. Epub 2023/03/31. <https://doi.org/10.1101/2023.03.13.23287179> PMID: 36993192.
32. Dewasurendra RL, Baniecki ML, Schaffner S, Siriwardena Y, Moon J, Doshi R, et al. Use of a *Plasmodium vivax* genetic barcode for genomic surveillance and parasite tracking in Sri Lanka. *Malar J*. 2020; 19(1):342. Epub 2020/09/23. <https://doi.org/10.1186/s12936-020-03386-3> PMID: 32958025.
33. WHO. Strategy for malaria elimination in the Greater Mekong Subregion (2015–2030). 2015:pp. 64.
34. Cui L, Yan G, Sattabongkot J, Cao Y, Chen B, Chen X, et al. Malaria in the Greater Mekong Subregion: heterogeneity and complexity. *Acta Trop*. 2012; 121(3):227–39. Epub 2011/03/09. <https://doi.org/10.1016/j.actatropica.2011.02.016> PMID: 21382335.
35. Geng J, Malla P, Zhang J, Xu S, Li C, Zhao Y, et al. Increasing trends of malaria in a border area of the Greater Mekong Subregion. *Malar J*. 2019; 18(1):309. Epub 2019/09/14. <https://doi.org/10.1186/s12936-019-2924-6> PMID: 31514740.
36. Cui L, Cao Y, Kaewkungwal J, Khamsiriwatchara A, Lawpoolsri S, Soe TN, et al. Malaria Elimination in the Greater Mekong Subregion: Challenges and Prospects. In: Manguin S, Dev V, editors. *Towards Malaria Elimination: A Leap Forward*. IntechOpen; 2018. p. 179–200.
37. Jitthai N. Migration and malaria. *Southeast Asian J Trop Med Public Health*. 2013; 44 Suppl 1:166–200; discussion 306–7. Epub 2013/10/29. PMID: 24159832.
38. Congpuong K, Ubalee R. Population genetics of *Plasmodium vivax* in four high malaria endemic areas in Thailand. *Korean J Parasitol*. 2017; 55(5):465–72. Epub 2017/11/07. <https://doi.org/10.3347/kjp.2017.55.5.465> PMID: 29103261.
39. Kittichai V, Koepfli C, Guitragool W, Sattabongkot J, Cui L. Substantial population structure of *Plasmodium vivax* in Thailand facilitates identification of the sources of residual transmission. *PLoS Negl Trop Dis*. 2017; 11(10):e0005930. Epub 2017/10/17. <https://doi.org/10.1371/journal.pntd.0005930> PMID: 29036178.
40. Li Y, Hu Y, Zhao Y, Wang Q, Ngassa Mbenda HG, Kittichai V, et al. Dynamics of *Plasmodium vivax* populations in border areas of the Greater Mekong sub-region during malaria elimination. *Malar J*. 2020; 19(1):145. Epub 2020/04/10. <https://doi.org/10.1186/s12936-020-03221-9> PMID: 32268906.

41. Parobek CM, Lin JT, Saunders DL, Barnett EJ, Lon C, Lanteri CA, et al. Selective sweep suggests transcriptional regulation may underlie *Plasmodium vivax* resilience to malaria control measures in Cambodia. *Proc Natl Acad Sci U S A*. 2016; 113(50):E8096–E105. Epub 2016/12/03. <https://doi.org/10.1073/pnas.1608828113> PMID: 27911780.
42. Snounou G, Viriyakosol S, Zhu XP, Jarra W, Pinheiro L, do Rosario VE, et al. High sensitivity of detection of human malaria parasites by the use of nested polymerase chain reaction. *Mol Biochem Parasitol*. 1993; 61(2):315–20. Epub 1993/10/01. [https://doi.org/10.1016/0166-6851\(93\)90077-b](https://doi.org/10.1016/0166-6851(93)90077-b) PMID: 8264734.
43. Diez Benavente E, Ward Z, Chan W, Mohareb FR, Sutherland CJ, Roper C, et al. Genomic variation in *Plasmodium vivax* malaria reveals regions under selective pressure. *PLoS One*. 2017; 12(5):e0177134. Epub 2017/05/12. <https://doi.org/10.1371/journal.pone.0177134> PMID: 28493919.
44. Purcell S, Neale B, Todd-Brown K, Thomas L, Ferreira MA, Bender D, et al. PLINK: a tool set for whole-genome association and population-based linkage analyses. *American journal of human genetics*. 2007; 81(3):559–75. <https://doi.org/10.1086/519795> PMID: 17701901.
45. Friedrich LR, Popovici J, Kim S, Dysoley L, Zimmerman PA, Menard D, et al. Complexity of Infection and Genetic Diversity in Cambodian *Plasmodium vivax*. *PLoS Negl Trop Dis*. 2016; 10(3):e0004526. Epub 2016/03/29. <https://doi.org/10.1371/journal.pntd.0004526> PMID: 27018585.
46. Galinsky K, Valim C, Salmier A, de Thoisy B, Musset L, Legrand E, et al. COIL: a methodology for evaluating malarial complexity of infection using likelihood from single nucleotide polymorphism data. *Malar J*. 2015; 14:4. Epub 2015/01/21. <https://doi.org/10.1186/1475-2875-14-4> PMID: 25599890.
47. Peakall R, Smouse PE. GenAIEx 6.5: genetic analysis in Excel. Population genetic software for teaching and research—an update. *Bioinformatics*. 2012; 28(19):2537–9. Epub 2012/07/24. <https://doi.org/10.1093/bioinformatics/bts460> PMID: 22820204.
48. Anderson TJ, Haubold B, Williams JT, Estrada-Franco JG, Richardson L, Mollinedo R, et al. Microsatellite markers reveal a spectrum of population structures in the malaria parasite *Plasmodium falciparum*. *Mol Biol Evol*. 2000; 17(10):1467–82. Epub 2000/10/06. <https://doi.org/10.1093/oxfordjournals.molbev.a026247> PMID: 11018154.
49. van Dorp L, Gelabert P, Rieux A, de Manuel M, de-Dios T, Gopalakrishnan S, et al. *Plasmodium vivax* Malaria Viewed through the Lens of an Eradicated European Strain. *Mol Biol Evol*. 2020; 37(3):773–85. Epub 2019/11/08. <https://doi.org/10.1093/molbev/msz264> PMID: 31697387.
50. Weir BS, Cockerham CC. Estimating F-Statistics for the Analysis Of Population Structure. *Evolution; international journal of organic evolution*. 1984; 38(6):1358–70. <https://doi.org/10.1111/j.1558-5646.1984.tb05657.x> PMID: 28563791.
51. Danecek P, Auton A, Abecasis G, Albers CA, Banks E, DePristo MA, et al. The variant call format and VCFtools. *Bioinformatics*. 2011; 27(15):2156–8. Epub 2011/06/10. <https://doi.org/10.1093/bioinformatics/btr330> PMID: 21653522.
52. Balloux F, Lugon-Moulin N. The estimation of population differentiation with microsatellite markers. *Mol Ecol*. 2002; 11(2):155–65. Epub 2002/02/22. <https://doi.org/10.1046/j.0962-1083.2001.01436.x> PMID: 11856418.
53. Chang CC, Chow CC, Tellier LC, Vattikuti S, Purcell SM, Lee JJ. Second-generation PLINK: rising to the challenge of larger and richer datasets. *GigaScience*. 2015; 4:7. <https://doi.org/10.1186/s13742-015-0047-8> PMID: 25722852.
54. Saitou N, Nei M. The neighbor-joining method: a new method for reconstructing phylogenetic trees. *Mol Biol Evol*. 1987; 4(4):406–25. <https://doi.org/10.1093/oxfordjournals.molbev.a040454> PMID: 3447015.
55. Kumar S, Stecher G, Tamura K. MEGA7: Molecular Evolutionary Genetics Analysis Version 7.0 for Bigger Datasets. *Mol Biol Evol*. 2016; 33(7):1870–4. Epub 2016/03/24. <https://doi.org/10.1093/molbev/msw054> PMID: 27004904.
56. Alexander DH, Novembre J, Lange K. Fast model-based estimation of ancestry in unrelated individuals. *Genome Res*. 2009; 19(9):1655–64. Epub 2009/08/04. <https://doi.org/10.1101/gr.094052.109> PMID: 19648217.
57. Ellis JA, Ong B. The MassARRAY((R)) System for Targeted SNP Genotyping. *Methods Mol Biol*. 2017; 1492:77–94. Epub 2016/11/09. https://doi.org/10.1007/978-1-4939-6442-0_5 PMID: 27822857.
58. Viriyakosol S, Siripoon N, Petcharapirat C, Petcharapirat P, Jarra W, Thaihong S, et al. Genotyping of *Plasmodium falciparum* isolates by the polymerase chain reaction and potential uses in epidemiological studies. *Bull World Health Organ*. 1995; 73(1):85–95. Epub 1995/01/01. PMID: 7704931.
59. Kirchgatter K, del Portillo HA. Molecular analysis of *Plasmodium vivax* relapses using the MSP1 molecule as a genetic marker. *J Infect Dis*. 1998; 177(2):511–5. Epub 1998/02/18. <https://doi.org/10.1086/517389> PMID: 9466551.

60. Cui L, Escalante AA, Imwong M, Snounou G. The genetic diversity of *Plasmodium vivax* populations. *Trends Parasitol.* 2003; 19(5):220–6. Epub 2003/05/24. [https://doi.org/10.1016/s1471-4922\(03\)00085-0](https://doi.org/10.1016/s1471-4922(03)00085-0) PMID: 12763428.
61. Cui L, Mascorro CN, Fan Q, Rzomp KA, Khuntirat B, Zhou G, et al. Genetic diversity and multiple infections of *Plasmodium vivax* malaria in Western Thailand. *Am J Trop Med Hyg.* 2003; 68(5):613–9. Epub 2003/06/19. <https://doi.org/10.4269/ajtmh.2003.68.613> PMID: 12812356.
62. Rungsihirunrat K, Chaijaroenkul W, Siripoon N, Seugorn A, Na-Bangchang K. Genotyping of polymorphic marker (MSP3alpha and MSP3beta) genes of *Plasmodium vivax* field isolates from malaria endemic of Thailand. *Trop Med Int Health.* 2011; 16(7):794–801. Epub 2011/03/31. <https://doi.org/10.1111/j.1365-3156.2011.02771.x> PMID: 21447062.
63. Daron J, Boissiere A, Boundenga L, Ngoubangoye B, Houze S, Arnathau C, et al. Population genomic evidence of *Plasmodium vivax* Southeast Asian origin. *Sci Adv.* 2021; 7(18). Epub 2021/04/30. <https://doi.org/10.1126/sciadv.abc3713> PMID: 33910900.
64. Zhao Y, Aung PL, Ruan S, Win KM, Wu Z, Soe TN, et al. Spatio-temporal trends of malaria incidence from 2011 to 2017 and environmental predictors of malaria transmission in Myanmar. *Infect Dis Poverty.* 2023; 12(1):2. Epub 2023/01/29. <https://doi.org/10.1186/s40249-023-01055-6> PMID: 36709318.
65. Xu JW, Lin ZR, Zhou YW, Lee R, Shen HM, Sun XD, et al. Intensive surveillance, rapid response and border collaboration for malaria elimination: China Yunnan's "3 + 1" strategy. *Malar J.* 2021; 20(1):396. Epub 2021/10/11. <https://doi.org/10.1186/s12936-021-03931-8> PMID: 34627264.
66. Lin ZR, Li SG, Sun XD, Guo XR, Zheng Z, Yang J, et al. Effectiveness of joint 3 + 1 malaria strategy along China-Myanmar cross border areas. *BMC Infect Dis.* 2021; 21(1):1246. Epub 2021/12/16. <https://doi.org/10.1186/s12879-021-06920-z> PMID: 34906092.
67. Hong NV, Delgado-Ratto C, Thanh PV, Van den Eede P, Guetens P, Binh NT, et al. Population Genetics of *Plasmodium vivax* in Four Rural Communities in Central Vietnam. *PLoS Negl Trop Dis.* 2016; 10(2):e0004434. Epub 2016/02/13. <https://doi.org/10.1371/journal.pntd.0004434> PMID: 26872387.
68. Imwong M, Nair S, Pukrittayakamee S, Sudimack D, Williams JT, Mayxay M, et al. Contrasting genetic structure in *Plasmodium vivax* populations from Asia and South America. *Int J Parasitol.* 2007; 37(8–9):1013–22. Epub 2007/04/20. <https://doi.org/10.1016/j.ijpara.2007.02.010> PMID: 17442318.
69. Auburn S, Benavente ED, Miotto O, Pearson RD, Amato R, Grigg MJ, et al. Genomic analysis of a pre-elimination Malaysian *Plasmodium vivax* population reveals selective pressures and changing transmission dynamics. *Nat Commun.* 2018; 9(1):2585. Epub 2018/07/04. <https://doi.org/10.1038/s41467-018-04965-4> PMID: 29968722.
70. Arnott A, Mueller I, Ramsland PA, Siba PM, Reeder JC, Barry AE. Global Population Structure of the Genes Encoding the Malaria Vaccine Candidate, *Plasmodium vivax* Apical Membrane Antigen 1 (PvAMA1). *PLoS Negl Trop Dis.* 2013; 7(10):e2506. Epub 2013/11/10. <https://doi.org/10.1371/journal.pntd.0002506> PMID: 24205419.
71. Luo Z, Sullivan SA, Carlton JM. The biology of *Plasmodium vivax* explored through genomics. *Ann N Y Acad Sci.* 2015; 1342:53–61. Epub 2015/02/20. <https://doi.org/10.1111/nyas.12708> PMID: 25693446.
72. Win AYN, Maung TM, Wai KT, Oo T, Thi A, Tipmontree R, et al. Understanding malaria treatment-seeking preferences within the public sector amongst mobile/migrant workers in a malaria elimination scenario: a mixed-methods study. *Malar J.* 2017; 16(1):462. Epub 2017/11/15. <https://doi.org/10.1186/s12936-017-2113-4> PMID: 29132373.
73. McMichael C, Healy J. Health equity and migrants in the Greater Mekong Subregion. *Glob Health Action.* 2017; 10(1):1271594. Epub 2017/04/30. <https://doi.org/10.1080/16549716.2017.1271594> PMID: 28452652.